Cellular/Molecular

Serotonin Disinhibits a *Caenorhabditis elegans* Sensory Neuron by Suppressing Ca^{2+}-Dependent Negative Feedback

Paul D.E. Williams, Jeffrey A. Zahratka, Matthew Rodenbeck, Jason Wanamaker, Hilary Linzie, and Bruce A. Bamber

Department of Biological Sciences, University of Toledo, Toledo, Ohio 43606-3390

Neuromodulators, such as serotonin (5-HT), alter neuronal excitability and synaptic strengths, and define different behavioral states. Neuromodulator-dependent changes in neuronal activity patterns are frequently measured using calcium reporters because calcium imaging can easily be performed on intact functioning nervous systems. With only 302 neurons, the nematode *Caenorhabditis elegans* provides a relatively simple, yet powerful, system to understand neuromodulation at the level of individual neurons. *C. elegans* hermaphrodites are repelled by 1-octanol, and the initiation of these aversive responses is potentiated by 5-HT. 5-HT acts on the ASH polymodal nociceptors that sense the 1-octanol stimulus. Surprisingly, 5-HT suppresses ASH Ca^{2+} transients while simultaneously potentiating 1-octanol-dependent ASH depolarization. Here we further explore this seemingly inverse relationship. Our results show the following (1) 5-HT acts downstream of depolarization, through $G\alpha_q$-mediated signaling and calcineurin, to inhibit L-type voltage-gated Ca^{2+} channels; (2) the 1-octanol-evoked Ca^{2+} transients in ASHs inhibit depolarization; and (3) the Ca^{2+}-activated K^+ channel, SLO-1, acts downstream of 5-HT and is a critical regulator of ASH response dynamics. These findings define a Ca^{2+}-dependent inhibitory feedback loop that can be modulated by 5-HT to increase neuronal excitability and regulate behavior, and highlight the possibility that neuromodulator-induced changes in the amplitudes of Ca^{2+} transients do not necessarily predict corresponding changes in depolarization.

Key words: *Caenorhabditis elegans*; Ca^{2+} inhibition; L-type Ca^{2+} channel; nociception; serotonin; SLO-1 BK channel

Significance Statement

Neuromodulators, such as 5-HT, modify behavior by regulating excitability and synaptic efficiency in neurons. Neuromodulation is often studied using Ca^{2+} imaging, whereby neuromodulator-dependent changes in neuronal activity levels can be detected in intact, functioning circuits. Here we show that 5-HT reduces the amplitude of depolarization-dependent Ca^{2+} transients in a *C. elegans* nociceptive neuron, through $G\alpha_q$ signaling and calcineurin but that Ca^{2+} itself inhibits depolarization, likely through Ca^{2+}-activated K^+ channels. The net effect of 5-HT, therefore, is to increase neuronal excitability through disinhibition. These results establish a novel 5-HT signal transduction pathway, and demonstrate that neuromodulators can change Ca^{2+} signals and depolarization amplitudes in opposite directions, simultaneously, within a single neuron.

Introduction

Neuromodulation is an important mechanism for regulating nervous system function and can generate behavioral flexibility in response to changing conditions (Marder, 2012). Major neuromodulatory neurotransmitters include the monoamines, such as serotonin and dopamine (Harris-Warrick and Johnson, 2010), and neuropeptides, for instance, oxytocin, vasopressin, and the opioid peptides (Stein and Zollner, 2009; Stoop, 2014). These molecules regulate neuronal excitability and synaptic strengths through G-protein signaling cascades, and can reconfigure neural circuits to produce differential outputs (Swensen and Marder, 2001; Harris-Warrick and Johnson, 2010; Gutierrez and Marder, 2014; Nadim and Bucher, 2014). Neuromodulatory signaling cascades are involved in many neurological conditions, including anxiety, depression, schizophrenia, chronic pain, and drug addiction, and drugs used to treat these conditions frequently act to increase or decrease neuromodulatory signaling (McCreary and Newman-Tancredi, 2015; Chiechio, 2016; Yohn et al., 2017).

Received July 5, 2017; revised Jan. 4, 2018; accepted Jan. 12, 2018.

Author contributions: P.D.E.W., J.A.Z., and B.A.B. designed research; P.D.E.W., J.A.Z., M.R., J.W., H.L., and B.A.B. performed research; P.D.E.W., J.A.Z., and B.A.B. analyzed data; P.D.E.W. and B.A.B. wrote the paper.

This work was supported by National Institutes of Health Grants R56 AI072644 and R15 AI109573. We thank the *C. elegans* Genetics Center for strains; Yifan Xu and Cornelia Bargmann for the kind gift of the ASH::GCaMP3 marker; Theodore Lindsay, Shawn Lockery, and Miriam Goodman for assistance with electrophysiology; William Schafer and James Cregg for assistance with the video microscopy setup; Amanda Korchnak for technical assistance; and Richard Komuniecki for valuable input.

The authors declare no competing financial interests.

Correspondence should be addressed to Dr. Bruce A. Bamber, Department of Biological Sciences, University of Toledo, 2801 W Bancroft Street, Toledo, OH 43606-3390. E-mail: Bruce.bamber@utoledo.edu.

DOI:10.1523/JNEUROSCI.1908-17.2018

 0270-6474/18/382069-12$15.00/0

Although neuromodulators and their receptors have been extensively catalogued over many years, neuromodulatory signaling is still not fully understood at the cellular or network levels. Whole-brain optical recording is a promising new approach to understand neuromodulation because, in principle, activity patterns can be compared in the presence and absence of neuromodulators, within intact nervous systems in freely behaving animals (Kato et al., 2015; Lemon et al., 2015; Poort et al., 2015; Naumann et al., 2016). Fluorescent Ca^{2+} sensors, such as the GCaMPs, are currently the reporters of choice, as their speed, sensitivity, and ease of expression are superior to alternatives such as fluorescent voltage indicators (Vogt, 2015). However, measurable Ca^{2+} levels provide an indirect indication of neuronal activation, with Ca^{2+} usually entering the cytoplasm through voltage-gated Ca^{2+} channels (VGCCs) that activate upon depolarization. As a consequence, overreliance on Ca^{2+} signals to analyze circuit function has three principal pitfalls: First, the activity of the voltage-gated Ca^{2+} channels can be modulated by intracellular signaling cascades, so the Ca^{2+} signal strength may reflect more the functional state of Ca^{2+} channel than the amplitude of the underlying depolarization. Second, Ca^{2+} may be released from intracellular stores independently of depolarization, leading to overestimation of neuronal activation. Third, Ca^{2+} itself is a potent signaling molecule with significant effects on the membrane potential, yet Ca^{2+} signals are often interpreted simply as passive indicators of membrane potential changes.

Caenorhabditis elegans is an excellent system to understand neuromodulation at single neuron resolution because its nervous system is relatively small and simple (only 302 neurons), stereotyped in development and structure, and fully reconstructed by serial section electron microscopy (White et al., 1986; Hobert, 2010). Moreover, they are transparent, which facilitates the use of optical reporters; in particular, Ca^{2+} imaging is widely used. Importantly, neuromodulators, receptors, and downstream signaling pathways are highly conserved between *C. elegans* and mammals (Chase and Koelle, 2007; Koelle, 2016). Aversive locomotory responses to the noxious odorant 1-octanol are potentiated by the neuromodulator 5-HT. 5-HT acts on the ASH polymodal nociceptive neurons (among others) to shorten the lag time between sensation and aversive reaction stimulated by 30% 1-octanol (Chao et al., 2004; Harris et al., 2011). We have begun addressing neuromodulatory mechanisms with an emphasis on Ca^{2+} signaling, using this relatively simple background. We previously showed that 5-HT reduces the ASH Ca^{2+} signal in response to 1-octanol, in apparent contradiction to the potentiated aversive behavior. However, direct electrical recordings showed that 5-HT treatment actually potentiates ASH depolarization (Zahratka et al., 2015). Here, we delineate the relationship between 5-HT signaling, Ca^{2+} transient amplitude, and modulation of depolarization, demonstrating that 5-HT potentiates ASH excitability by suppressing a Ca^{2+}-dependent inhibitory feedback loop. These findings highlight potential nonlinearities in the relationship between Ca^{2+} signal amplitudes and depolarization amplitudes that may significantly distort the interpretation of circuit analysis data.

Materials and Methods

Strains and constructs. Strains were maintained on NGM agar plates with *Escherichia coli* OP50 bacteria per standard protocols. Strains used were as follows: N2, FY908 *grls17* [*Psra-6::GCaMP3*], FY928 *grls17* [*Psra-6::GCaMP3*]; *Pgpa-4::RFP*, FY867 *ser-5 (tm2654) I;kyEx2865* [*Psra-6::GCaMP3*], FY934 *egl-30 (n686sd) I; grls17* [*Psra-6::GCaMP3*], FY936 *slo-1 (eg142) V; grls17* [*Psra-6::GCaMP3*], FY975 *tax-6 (p675) IV; grls17* [*Psra-6::GCaMP3*]. Neuron-specific RNAi transgenes were generated as previously described (Esposito et al., 2007) and coinjected with *Punc-122::RFP* at a concentration of 50 ng/μl. Animals were analyzed within three generations of original injection. The primers used to produce the *Psra-6::slo-1 RNAi* transgene were as follows: Psra-6 promoter forward: 5′-CACTGATGTACCTTTCTATCTTTCTAAAC-3′; Psra-6 promoter forward internal: 5′-CTTTCTATCTTTCTAAACTTTGG-3′; slo-1 transcript forward: 5′-CGTACCAGAAATTGCCGATTTG-3′; slo-1 transcript forward internal: 5′-CCGATTTGATTGGAAACCGG-3′; slo-1 transcript reverse: 5′-CTGCTAAGATCCAGAGAATC-3′; slo-1 transcript reverse internal: 5′-CCAGAGAATCCATGACAGTC-3′; Psra-6::slo-1 promoter reverse sense: 5′-CAATTTCTGGTACGGGCAAAATCTGAAATAATAAATATTAAATTCTGCG-3′; and Psra-6::slo-1 promoter reverse antisense: 5′-ATCTTAGCAGGGCAAAATCTGAAATAATAAATATTAAATTCTGCG-3′.

Calcium imaging. Calcium imaging experiments were performed as previously described (Mills et al., 2012; Zahratka et al., 2015). Animals were glued to a 15-mm-diameter circular coverslip coated with Sylgard (Dow Corning), immersed in external solution (see below) using Worm-Glu cyanoacrylate glue (GluStitch, Delta). The coverslips were placed in a laminar flow chamber (Warner RC26G, Warner Instruments) and perfused continuously with external solution. External solution contained 150 mM NaCl, 5 mM KCl, 5 mM $CaCl_2$, 1 mM $MgCl_2$, 10 mM glucose, 15 mM HEPES, pH 7.30, 327–333 mOsm. 1-Octanol (~2.37 μM in external solution) was delivered under gravity feed through solenoid valves using a perfusion pencil (AutoMate Scientific) or homemade equivalent. All solutions contained the fluorescent tracer Sulforhodamine 101 (SR101, 1 μM), which stained the animals on contact and allowed visual inspection of flow. Solutions were delivered using the perfusion pencil as described above, mounted on a SF77B Perfusion Fast Step device (step size 200 μM, Warner Instruments) to provide precise computer control of pipette position. After each exposure, animals were visually examined for SR101 staining to confirm successful application and flow. No response was observed in ASHs to external solution containing 1 μM SR101 alone or in the ASIs (also expressing the *Psra-6::GCaMP3* reporter transgene).

Ca^{2+} imaging of ASH neurons via high K^+ stimulation required partial dissection to expose the ASHs to the external solution. Dissection was performed as described previously (Goodman et al., 1998). The cuticle was slit with a patch pipette (TW150–3, World Precision Instruments) that had been melted at the tip, drawn to a fine point, and broken back to create a sharp-ended "cutter," using an MF-83 microforge (Narishige). Cutters were mounted on a micromanipulator (MP285, Sutter instruments) to puncture the cuticle. A successful dissection would invariably expose only one ASH neuron, leaving the other within the cuticle, allowing exposed and unexposed ASH Ca^{2+} responses to be compared (see Fig. 6*D*). This dissection technique, and the validation of differential exposure of the two ASHs, is demonstrated in Movie 1. Exposure times were 110 ms with 4× binning. High K^+ (30 mM) external solution contained 120 mM NaCl, 30 mM KCl, 5 mM $CaCl_2$, 1 mM $MgCl_2$, 10 mM glucose, 15 mM HEPES, pH 7.30, 327–333 mOsm, and was applied via a four-barreled glass puffer (barrel cross section 300 μm), mounted on a SF77B Perfusion Fast Step device (Warner Instruments). Solutions were delivered using a syringe pump (KD Scientific) at a rate of 0.2 ml/min. All recordings were performed on an Axioskop 2 FS Plus upright compound microscope (40× Achroplan water-immersion objective, GFP filter set #38), fitted with an Orca ER CCD camera (Hamamatsu) and an automated shutter (Uniblitz, Vincent Associates). Minimal illumination intensity was used to prevent GCaMP3 photobleaching, and we did not observe differential photobleaching rates between different genotypes and treatment groups.

Cyclosporin A (CsA) exposure was achieved by incubating animals on NGM containing 50 μM CsA for 45 min. 5-HT and nemadipine-A (NemA) exposure was performed using one of two methods: incubation on NGM plates or direct application. 5-HT incubation was performed on 4 mM 5-HT-containing NGM plates for 30 min. NemA incubation was performed on 5 μM NemA-containing NGM plates for 45 min. CsA, 5-HT, and NemA plates were prepared fresh on each day of recording. Direct application of 5-HT and NemA was achieved using a two-opening theta (Θ) glass tube that had been heated and drawn to a fine point by hand. Two lengths of PE10 polyethylene tubing (0.61OD × 0.28ID)

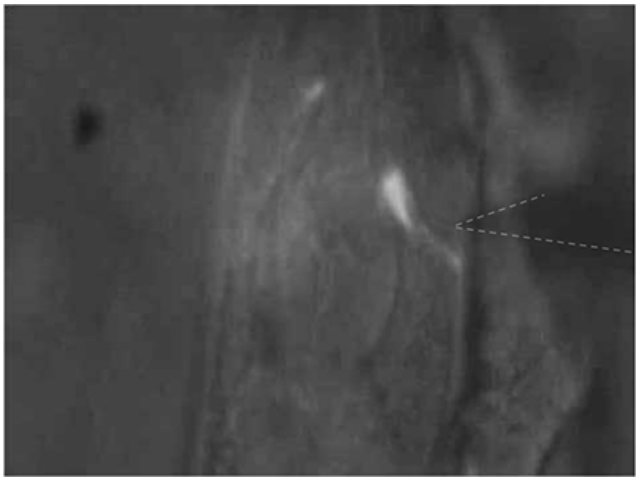

Movie 1. Differential dissection of ASHR and ASHL. Successful dissection of ASHR. Using a glass pipette sharpened to a fine point (see Materials and Methods), the cuticle is punctured just caudal to the ASHR soma, taking care to avoid the axon. ASHR can then be seen to extrude itself through the cuticle breach, becoming exposed to the external solution, without fragmentation of the soma or processes. ASHL remains within the cuticle, near its original position. Focal plane is varied before and after dissection to emphasize displacement of ASHR in the vertical dimension following dissection. Frame rate ~10 Hz.

(Warner) were inserted into the back of the theta glass and sealed using Sylgard. A control stream (external solution) occupied one line, and a drug containing solution occupied the second. Solutions were delivered via a syringe pump (KD Scientific) at a rate of 0.05 ml/min. Supply lines were activated or inactivated manually using nylon three-way Luer Lock stopcocks; only one line was active at any time. Both streams from this dual-chambered pipette were capable of shielding the exposed ASH cell body from the 1-octanol stream perfusing the amphid (see Fig. 2*A*). Animals were inspected for SR101 staining after each 1-octanol application, and any animal whose neuron had become exposed to the 1-octanol stream was discarded. 5-HT dose–response curves were generated using the equation, $A = A_{max}/(1 + 10^{(\mathrm{LogEC50\text{-}[agonist]}) \times n)})$, where A is the percentage of inhibition of the Ca^{2+} signal at a given 5-HT concentration, A_{max} inhibition of the Ca^{2+} signal at 5-HT saturation, EC_{50} of 5-HT is the concentration necessary to elicit half-maximal inhibition of the 1-octanol induced Ca^{2+} signal, and n is the slope coefficient. Curve fitting was performed using GraphPad Prism software. Fluorescent images were acquired using MetaVue 7.6.5 (MDS Analytical Technologies), and analyzed with Jmalyze software (Rex Kerr). Exposure times were 50 ms with 4× binning. We routinely compared baseline fluorescence values between mutant or drug-treated worms and corresponding controls.

Electrophysiology. For patch-clamp analysis, animals were glued and placed in the recording chamber as described above. ASH cell bodies (identified by GCaMP3 expression and lack of RFP expression, ASI *Pgpa-4::RFP*) were exposed for whole-cell recordings by slitting the cuticle as described above. Dissection quality was validated by visually inspecting the dendrite of the exposed ASH to ensure it had not been severed. Whole-cell recordings were performed as previously described (Zahratka et al., 2015). Briefly, we used pressure-polished patch pipettes (Goodman and Lockery, 2000) with 12–25 MΩ resistance containing low Cl^- internal solution (15 mM KCl, 115 mM K gluconate, 10 mM HEPES, 5 mM $MgCl_2$, 0.25 mM $CaCl_2$, 5 mM EGTA, 20 mM sucrose, 5 mM MgATP, 0.25 mM NaGTP, pH 7.20, 315 mOsm). 1-Octanol was delivered as described above via perfusion pencil mounted on SF77B Perfusion Fast Step Device (step size 200 μM, Warner Instruments). NemA was delivered using the dual-chambered pipette, as previously described. Cells were observed after each 1-octanol application using SR101. Any cell that had become exposed directly to the 1-octanol stream was discarded. Signals were recorded with an Axopatch 200B amplifier (Molecular Devices) in current-clamp mode (0 pA injected current, 10 kHz sampling, 2 kHz filtering), digitized with a Digidata 1440A digitizer, and analyzed using pCLAMP10 software (Molecular Devices).

Behavioral assays. Behavioral responses to 1-octanol were assayed as previously described (Chao et al., 2004; Harris et al., 2009). Twenty to 40 L4 animals were picked the night before the assay onto fresh OP50-seeded NGM plates. 5-HT-containing plates were prepared the day of the assay 2 h before the experiment by adding 4 mM 5-HT creatinine sulfate monohydrate to molten agar (~55°C). 1-Octanol was presented to a forward moving animal via a glass capillary that was dipped in 30% 1-octanol solution (dissolved in 100% ethanol, v/v). For assays in the absence of 5-HT, animals were transferred from the stock plate to an intermediate plate for 1 min to remove any OP50, and transferred to a food-free assay plate, and tested 10 min later. In contrast, 5-HT-assayed animals were transferred to the 5-HT containing plates after the intermediate plate and tested 30 min later.

All reagents were obtained from Fisher Scientific or Sigma-Aldrich.

Experimental design and statistical analysis. For Ca^{2+} imaging and electrophysiology experiments, a minimum of 5 young hermaphrodite adult animals were recorded for each treatment/mutation for each day of recording. For behavioral experiments, a minimum of 25 young hermaphrodite adult animals were needed for each treatment/mutation analyzed. All experiments were performed between 19°C and 23°C. All reagents were made fresh on the day of the experiment.

Statistical analysis was performed using two-tailed Student's t tests (unpaired unless indicated otherwise), one-way ANOVA with Tukey post test, and repeated-measures ANOVA with Tukey post test. All data are presented as mean ± SEM using GraphPad Prism software.

Results

5-HT acts downstream of depolarization to reduce the stimulus-induced Ca^{2+} transient in ASH

5-HT reduces the ASH Ca^{2+} signal, but the mechanism is unclear (Zahratka et al., 2015). 5-HT is unlikely to reduce the initial sensory potential because overall ASH depolarization is enhanced (Zahratka et al., 2015); therefore, we have hypothesized that 5-HT modulates Ca^{2+} dynamics downstream of the initial 1-octanol-dependent depolarization. To test this idea, we determined whether 5-HT could reduce Ca^{2+} transients in ASHs after artificial depolarization induced by elevated $[K^+]$ treatment (30 mM compared with 5 mM, after partial dissection to expose the ASH soma to the bath; see Materials and Methods). High K^+ treatment led to robust Ca^{2+} transients, which were sensitive to the L-type Ca^{2+} channel blocker NemA, as observed previously for 1-octanol-dependent ASH Ca^{2+} transients (Fig. 1*A*,*B*) (Zahratka et al., 2015). 5-HT treatment significantly inhibited high K^+ ASH Ca^{2+} transients similar to 1-octanol treatment (Fig. 1*A*,*B*) (Zahratka et al., 2015). Similarly, 5-HT modulation of both high K^+- and 1-octanol-dependent signals are dependent on the 5-HT receptor SER-5 and the $G\alpha_q$ subunit EGL-30 to which it is coupled (Fig. 1*C*,*D*) (Zahratka et al., 2015). Together, these data suggest that 5-HT acts downstream of the initial ASH depolarization evoked by aversive olfactory stimuli to directly reduce Ca^{2+} transient amplitudes via a $G\alpha_q$-coupled pathway.

5-HT modulates ASH function at physiological concentrations and time scales

To further study 5-HT signaling in ASHs, we developed methods to apply 5-HT with precise control over concentration and time course. Monoamine studies in *C. elegans* have previously been performed by incubating worms on agar plates containing high (i.e., mM) concentrations of monoamines for ≥30 min (Chao et al., 2004; Harris et al., 2009, 2011; Ezcurra et al., 2011; Ghosh et

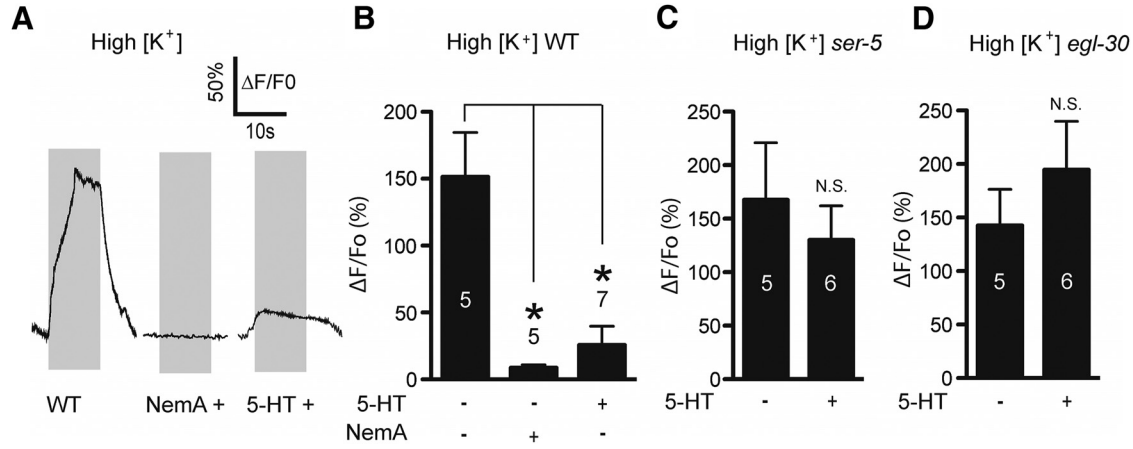

Figure 1. 5-HT inhibits Ca^{2+} signals downstream of depolarization. ***A***, Ca^{2+} responses in wild-type dissected ASHs exposed to high K^+ buffer: untreated (left trace), NemA-treated (middle trace), and 5-HT-treated (right trace). ***B***, Quantification of NemA and 5-HT inhibition of high K^+ amplitudes. *Significantly different from control ($F_{(2,15)} = 9.011$, $p = 0.0027$, ANOVA). ***C***, Loss of *ser-5* signaling prevents 5-HT inhibition of ASH Ca^{2+} in response to artificial depolarization. N.S., Not significantly different compared with untreated control ($p = 0.5456$, $t = 0.6281$, df = 9, unpaired *t* test). ***D***, Loss of the $G\alpha_q$ protein *egl-30* prevents 5-HT inhibition of high K^+ responses. N.S., Not significantly different compared with untreated control ($p = 0.3971$, $t = 0.8891$, df = 9, unpaired *t* test). Numbers in/above bars indicate *n*. Gray boxes represent duration of high K^+ exposure. Data are mean ± SEM.

al., 2016). Under these conditions, the effective concentration of ligand at the relevant receptors cannot be known or precisely controlled, and is affected by multiple factors, such as cuticular permeability, slow diffusion kinetics, and transport/degradation dynamics within the worm. We again turned to limited dissection to expose the ASH cell bodies to the bath, and applied 5-HT using a perfusion system that permitted ligand exchange over the course of a few seconds (see Materials and Methods; Fig. 2*A*). Importantly, this system was configured to perfuse the worm's nose and exposed neuronal soma independently, with no cross-contamination, so odorants can be applied to the nose while modulators are applied to the cell body (neurons directly exposed to 1-octanol showed rapid irreversible increases in Ca^{2+}, often followed by cellular fragmentation, suggesting that direct 1-octanol contact kills exposed cells). Under these conditions, the EC_{50} for 5-HT inhibition of 1-octanol-induced Ca^{2+} signals was calculated to be 6 nM (Fig. 2*B*) after a 1 min exposure time; 10 nM 5-HT was used in subsequent experiments, which produced a robust and reversible effect (Fig. 2*C*).

In the canonical $G\alpha_q$ pathway, phospholipase C activation leads to the production of diacylglycerol and inositol trisphosphate (IP_3), which binds to the IP_3 receptor and gates the release of Ca^{2+} from intracellular stores (Singer et al., 1997; Miller et al., 1999; Walker et al., 2009; Baker et al., 2013). We observed a rapid increase in GCaMP3 fluorescence upon 5-HT treatment that is SER-5-dependent, consistent with release of intracellular Ca^{2+} downstream of $G\alpha_q$ activation (Fig. 2*D*,*E*). NemA treatment did not significantly reduce the 5-HT-stimulated Ca^{2+} transient (Fig. 2*E*), consistent with an intracellular origin for this Ca^{2+}, rather than extracellular through EGL-19.

To determine whether this Ca^{2+} signal is functionally coupled to the inhibition of 1-octanol-induced Ca^{2+} responses in ASHs, we performed limited dissection to expose an ASH neuron, then sequentially treated the worm with 1-octanol (at the tip of the nose), 5-HT (at the ASH soma), and finally, in the continued presence of 5-HT, 1-octanol again. In the wild-type, 1-octanol generated a robust signal, 5-HT induced a somewhat smaller Ca^{2+} signal, and the second 1-octanol application generated a greatly reduced signal relative to the first (Fig. 2*F*, top, *G*, white bars), consistent with 5-HT inhibiting the 1-octanol response, as previously observed (Zahratka et al., 2015). In *ser-5* mutants, as expected, 5-HT alone did not induce a Ca^{2+} signal, and the second 1-octanol responses was unaffected (Fig. 2*F*, bottom, *G*, black bars). These results suggest that 5-HT activates a SER-5- and $G\alpha_q$-dependent signaling pathway, including release of Ca^{2+} from intracellular stores, to inhibit Ca^{2+} transients associated with 1-octanol stimulation in ASH neurons. Furthermore, 5-HT signaling is rapid, is reversible, and occurs at physiological 5-HT concentrations (i.e., comparable with 5-HT receptors in heterologous cells and neurons from other species) (Adolph and Tuan, 1972; Bunin and Wightman, 1998).

Calcineurin mediates 5-HT inhibition of 1-octanol induced Ca^{2+} signals

In cardiomyocytes, L-type VGCCs are inhibited through the calcium-dependent inhibition (CDI) pathway, where Ca^{2+}-calmodulin (CaM) binds to and activates calcineurin (CaN), which in turn dephosphorylates the channel at a conserved serine residue. CaM binding to a conserved IQ domain on the intracellular cytoplasmic tail of the channel is necessary for CaN dephosphorylation of its target serine (Blaich et al., 2012; Wang et al., 2014). In neurons, a CDI-like mechanism operates downstream of $G\alpha_q$-coupled GPCRs, with IP_3-R-dependent Ca^{2+} release activating CaM-CaN, which dephosphorylates and inactivates the L-type VGCC at the same serine residue (Hernandez-Lopez et al., 2000; Day et al., 2002; Stevens et al., 2003; Oliveria et al., 2012). The L-type VGCC forms a signaling complex with the IP_3-R through Shank and Homer, allowing the GPCR to control the L-type VGCC at extremely short range (Olson et al., 2005). The EGL-19 L-type VGCC in *C. elegans* also contains the conserved IQ domain and serine residue (Fig. 3*A*) and may associate with the IP_3-R directly through Ce-SHANK (SHN-1) (Oh et al., 2011). Therefore, we hypothesized that 5-HT activates a CDI-like pathway to regulate Ca^{2+} influx in ASH neurons, and predicted that CaN would be required for 5-HT signaling (outlined in Fig. 3*B*). CsA inhibits CaN in *C. elegans* (Bandyopadhyay et al., 2002; Donohoe et al., 2009). We preincubated worms in 50 μM CsA on agar plates for 45 min, performed partial dissection to expose ASHs to the bath, and repeated the sequential 1-octanol and 5-HT application protocol performed earlier (Fig. 3*C*,*D*). The initial 1-octanol response and the direct 5-HT responses were unaffected by CsA treatment. However, the second 1-octanol re-

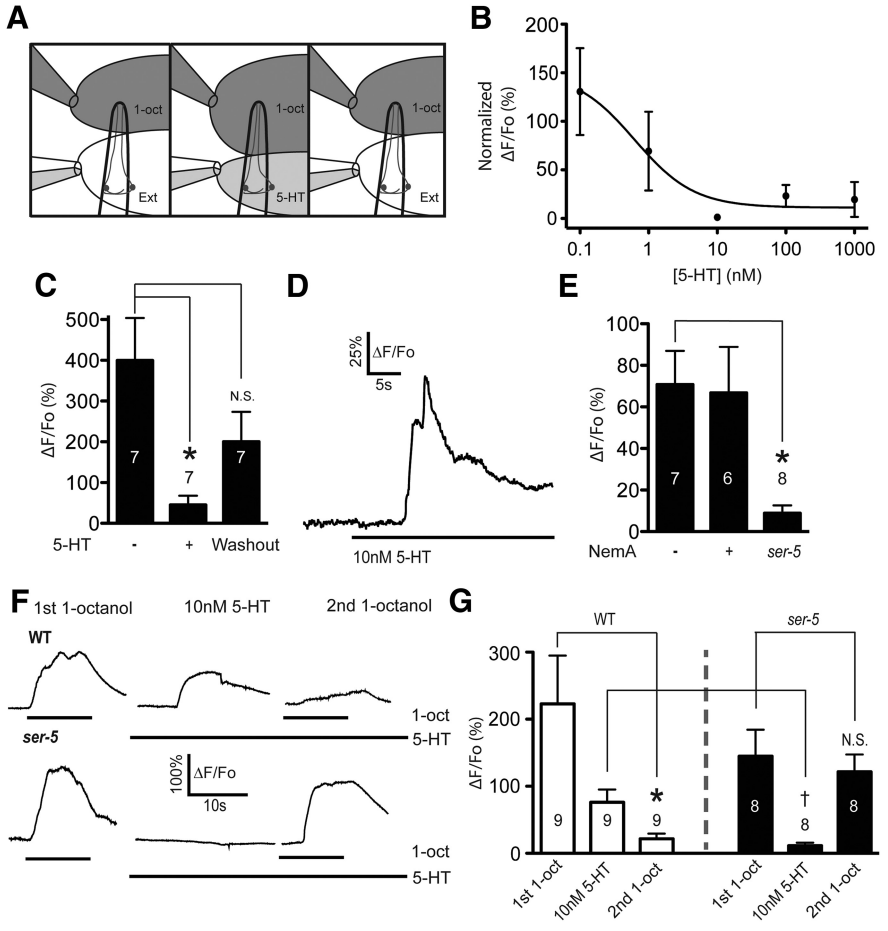

Figure 2. 5-HT modulation of ASH Ca^{2+} responses is potent, rapid, reversible, and involves release of Ca^{2+} from internal stores. ***A***, Diagram illustrating dual-pipette perfusion system. Left, Upper pipette delivers the olfactory stimulus, which is a saturated solution of 1-octanol (1-oct) in external solution. Pipette is mounted on a motorized drive, which can be moved to deliver stimuli at precise intervals. Lower pipette delivers external solution (ext) and deflects the 1-octanol solution away from the exposed cell body. The lower pipette contains a glass septum that separates two independent buffers, allowing rapid switching between them (e.g., ext alone, or ext + 5-HT) (middle, right). ***B***, Titration curve for 5-HT inhibition of the 1-octanol-evoked Ca^{2+} responses. ***C***, The 10 nM 5-HT (1 min exposure) inhibits 1-octanol induced Ca^{2+} responses, reversible after 5 min washout. *Significantly different from control ($F_{(2,6)} = 8.344$, $p = 0.0054$, repeated-measures ANOVA). N.S., Not significantly different from control. ***D***, Representative trace of 5-HT-induced Ca^{2+} signal in ASHs. ***E***, Ca^{2+} transient evoked by 10 nM 5-HT is NemA-insensitive and *ser-5*-dependent. *Significantly different from control ($F_{(2,18)} = 6.119$, $p = 0.0094$, ANOVA). ***F***, Representative traces of sequential 1-octanol and 5-HT exposures. Left, Initial 1-octanol-stimulated Ca^{2+} response. Middle, The 10 nM 5-HT-stimulated Ca^{2+} response. Right, Second 1-octanol-stimulated Ca^{2+} signals. Top, Wild-type. Bottom, *ser-5*. Bar below trace represents duration of ligand exposure. ***G***, Amplitudes of initial 1-octanol, 5-HT, and second 1-octanol responses in wild-type (white bars) and *ser-5* (black bars). *Significantly different from control (10 nM 5-HT second 1-octanol response vs untreated, $p = 0.0214$, $t = 2.852$, df = 8, paired *t* test). 5-HT responses in *ser-5* are significantly smaller than wild-type. †Significantly different from control (10 nM treated *ser-5* vs 10 nM 5-HT treated WT, $p = 0.0175$, $t = 2.722$, df = 13). N.S., Not significantly different from untreated control. Numbers in/above bars indicate *n*. For titration curve, $n = 4$ or 5 for each concentration. Data are mean ± SEM.

sponse was equal in amplitude to the first (Fig. 3*C*,*D*). These results show that CaN inhibition blocks the 5-HT-dependent diminution of ASH Ca^{2+} responses, suggesting that CaN acts downstream of Ca^{2+} in the 5-HT signaling pathway. Importantly, this result also shows that diminution of the second 1-octanol response after 5-HT application is unlikely to reflect a nonspecific ceiling effect in the ER Ca^{2+} releasing capacity (i.e., ER Ca^{2+} contributes to 1-octanol responses (Zahratka et al., 2015), and 5-HT-dependent Ca^{2+} release could deplete the ER of Ca^{2+}, leading to a diminished signal). In the presence of CsA, the second 1-octanol application still evoked a robust Ca^{2+} transient despite the earlier 5-HT-dependent Ca^{2+} release (Fig. 3*C*,*D*), which is incompatible with a ceiling effect explanation. CaN is also required for 5-HT modulation of Ca^{2+} responses evoked by high K^+ buffer. 5-HT did not inhibit these Ca^{2+} responses in the presence of CsA (Fig. 4*A*–*C*) or in *tax-6* mutants, which lack CaN (Kuhara et al., 2002) (Fig. 4*D*). Together, these results are consistent with TAX-6/CaN inhibiting Ca^{2+} entry into ASHs through its conserved ability to dephosphorylate the EGL-19 L-type VGCC. However, we cannot rule out that other targets of TAX-6/CaN could be playing a role, as this phosphatase has a wide substrate specificity (Bandyopadhyay et al., 2002).

Ca^{2+} inhibits ASH depolarization

How can 5-HT suppress stimulus-induced Ca^{2+} transients while simultaneously potentiating depolarization in ASHs? One possibility is that Ca^{2+} itself may act as a second messenger to inhibit depolarization, and if so, pharmacological block of L-type Ca^{2+} channels should potentiate depolarization. L-type channels are the predominant Ca^{2+} channel mediating somal Ca^{2+} influx in ASHs (Zahratka et al., 2015). To test this prediction, we performed direct electrophysiological recordings of ASH neurons, predicting that NemA inhibition of L-type voltage-gated Ca^{2+} channels should increase depolarization amplitude. Interestingly, after 45 min incubation on agar plates containing 5 μM NemA, resting membrane potentials in ASHs were highly unstable relative to untreated animals (Fig. 5*A*), which, unfortunately, precluded measurement of 1-octanol evoked depolarization. This observation is consistent with observations in other systems where blockade of L-type Ca^{2+} channels disrupts normal cellular physiology, resulting in rapid changes in ion channel expression, which could presumably affect the stability of the resting membrane potential (Hogan, 2007; Ransdell et al., 2012). To circumvent this difficulty, we performed partial dissection and acutely treated dissected ASHs with NemA for 60 s, before performing electrophysiological recordings. We first titrated NemA using 1-octanol evoked Ca^{2+} signals as a readout, and determined that 100 nM NemA consistently inhibited the channel (10 nM was also effective, but more variable; Fig. 5*B*). Baseline membrane potentials of these NemA-treated ASH neurons were stable; and most importantly, 1-octanol evoked depolarization was significantly potentiated (Fig. 5*C*,*D*). This result was particularly interesting, as Ca^{2+} entering through the L-type VGCCs is often assumed to be a primary carrier of inward current during depolarization. To verify that another VGCC (e.g., UNC-2 or CCA-1) was not activating to compensate, we carefully imaged the entire length of the ASH neuron during 1-octanol stimulation in the presence of NemA. We observed no increased Ca^{2+} signal in any ASH compartment (i.e., cilium, dendrite, soma or axon), and significant reduction of Ca^{2+} signals in the soma and dendrite (Fig. 5*E*). This result suggests that optically detectable Ca^{2+} influxes across the plasma membrane of the dendrite, soma, or axon are not the pri-

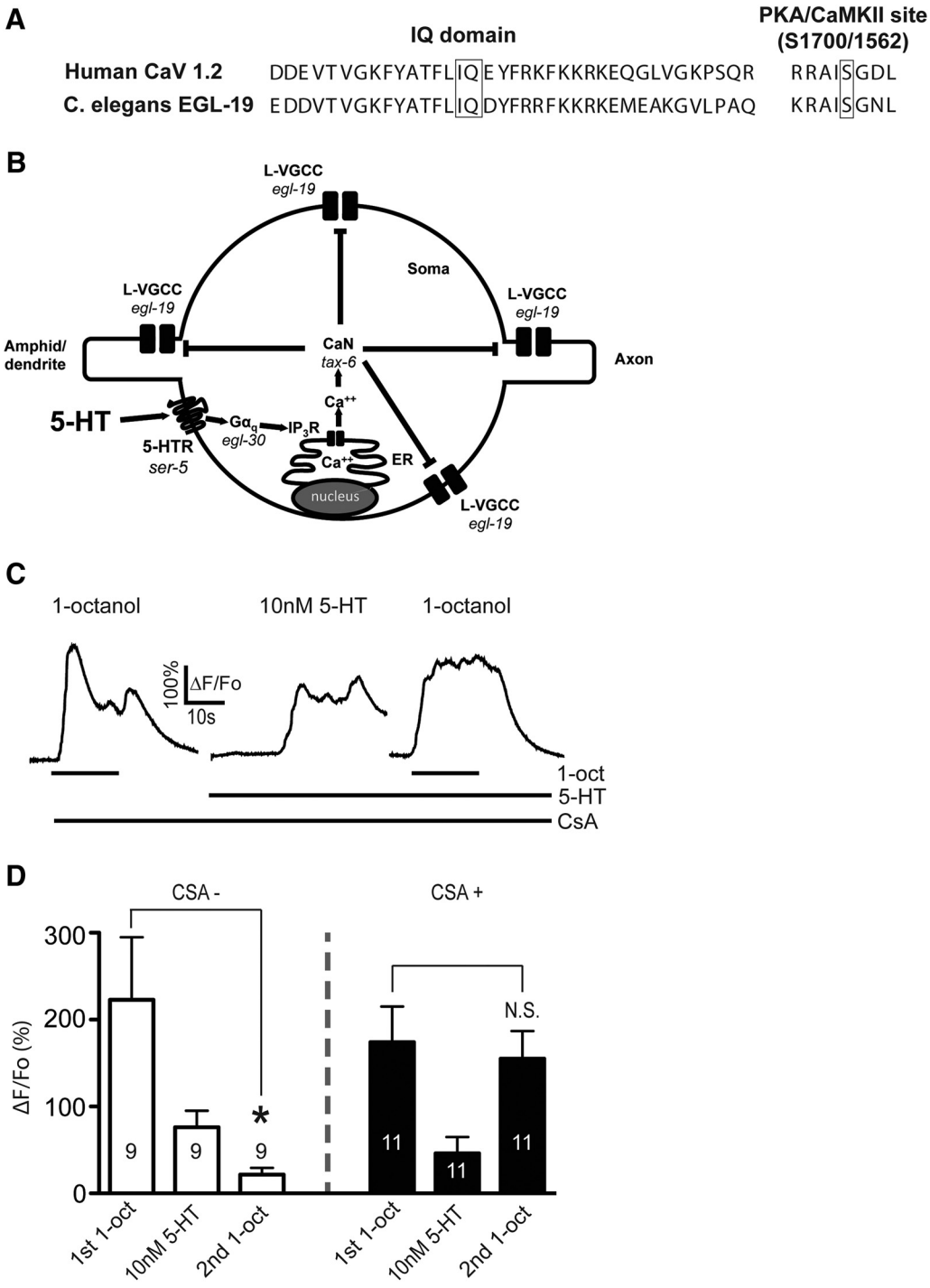

Figure 3. CaN is required for 5-HT inhibition of 1-octanol-evoked Ca^{2+} signals in ASHs. ***A***, The conserved IQ domain and the calcineurin dephosphorylation site are present in the *C. elegans* EGL-19 L-VGCC (human CaV 1.2 sequences shown for comparison). ***B***, Hypothesized signaling pathway in which 5-HT activates $G\alpha_q$ signaling, Ca^{2+} release from intracellular stores, calcineurin (TAX-6/CaN) activation, and inhibition of the EGL-19 L-type VGCC. ***C***, Representative traces of sequential 1-octanol and 5-HT exposures of CsA-treated worms. Left, Initial 1-octanol-stimulated Ca^{2+} response. Middle, 5-HT-stimulated Ca^{2+} response. Right, Second 1-octanol-stimulated Ca^{2+} signal. Bar below trace represents duration of ligand exposure. ***D***, Amplitudes of initial 1-octanol, 5-HT, and second 1-octanol responses in untreated wild-type (white bars, reproduced from Fig. 2*G*). *Significantly different from control (10 nM 5-HT-treated second 1-octanol response vs untreated, $p = 0.0214$, $t = 2.852$, df = 8, paired *t* test) and CsA-treated wild-type ASHs (black bars). N.S., Not significantly different from control. CsA treatment does not significantly change 5-HT-evoked Ca^{2+} signals ($p = 0.2814$, $t = 1.111$, df = 18). Numbers in/above bars indicate *n*. Data are mean ± SEM.

mary carriers of inward current during ASH depolarization. Together with the previous results, we conclude that ASH intracellular Ca^{2+} exerts negative feedback on depolarization and that 5-HT disinhibits ASHs by suppressing this feedback.

SLO-1 is required in ASHs for 5-HT signaling and regulation of olfactory response dynamics

The SLO-1 voltage- and Ca^{2+}-activated K^+ channel (homologous to the mammalian BK channel) is expressed throughout the

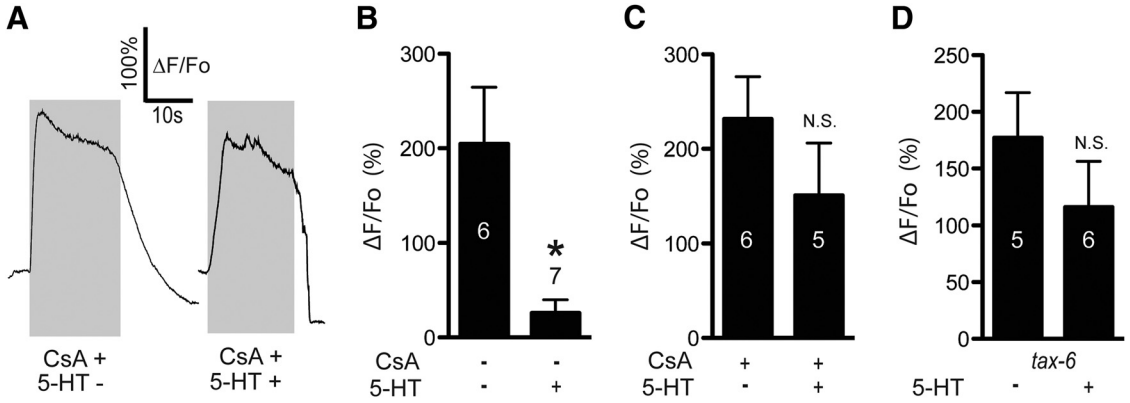

Figure 4. CaN is required for 5-HT inhibition of high K^+-evoked Ca^{2+} signals in ASHs. ***A***, Representative traces of high K^+-stimulated Ca^{2+} transients in CsA-treated ASHs. 5-HT treatment (10 nM) as indicated. ***B***, Quantitative comparison of 5-HT inhibition (data reproduced from Fig. 1*B*). *Significantly different from control (5-HT treated vs untreated, $p = 0.0030$, $t = 3.89$, df = 10). ***C***, Ca^{2+} amplitudes in CsA-treated ASHs in the absence and presence of 5-HT. N.S., Not significant from untreated counterpart ($p = 0.2790$, $t = 1.152$, df = 9). ***D***, 5-HT inhibition of high K^+-induced Ca^{2+} signals *tax-6* mutants. N.S., Not significantly different from untreated counterpart ($p = 0.3146$, $t = 1.065$, df = 9). Number in/above bars indicates *n*. Data are mean ± SEM.

C. elegans nervous system (Wang et al., 2001) and could potentially mediate Ca^{2+}-dependent inhibition of depolarization in ASHs (Goodman et al., 1998). We used various genetic manipulations to investigate a possible role for SLO-1 in ASH signaling and modulation. ASH-specific RNAi knockdown of SLO-1 prevented 5-HT potentiation of 1-octanol aversive responses, demonstrating a key role for SLO-1 in the 5-HT signaling pathway within ASHs (Fig. 6*A*). Similarly, *slo-1* loss-of-function mutants were also 5-HT insensitive, corroborating the RNAi result (Fig. 6*A*).

Next, we observed that the kinetics of the 1-octanol-induced Ca^{2+} responses in ASHs were much less uniform and consistent in the absence of SLO-1 (Fig. 6*B*,*C*). This effect was most readily observed and quantified by comparing the traces from the left ASH (ASHL) and the right ASH (ASHR) in the same animal, recorded simultaneously. In wild-type, ASHL and ASHR responded with nearly identical kinetics; this uniformity led to Pearson's correlation coefficients (between ASHL and ASHR signals) approaching 1.0 (Fig. 6*B*,*C*). By contrast, *slo-1* mutants and ASH-specific RNAi animals showed highly irregular response profiles (representative examples shown), resulting in significant asynchrony between ASHL and ASHR, with significantly reduced Pearson's coefficients (Fig. 6*B*,*C*). This finding suggests that the remarkable uniformity of ASH Ca^{2+} response kinetics is the result of intrinsic ionic mechanisms critically dependent on SLO-1, and that these mechanisms are powerful enough to produce bilaterally symmetric responses in the two ASH neurons, which is a novel insight into *C. elegans* sensory neurophysiology.

However, it is also possible that ASHL and ASHR are electrically coupled because a single gap junction was observed between ASHL and ASHR by electron microscopy (White et al., 1986). This coupling may be somehow dependent on SLO-1, possibly developmentally (Alqadah et al., 2016), and therefore lost in the *slo-1* mutants. To distinguish these possibilities, we once again partially dissected single wild-type ASHs (see Materials and Methods; Movie 1) and stimulated them with high K^+ buffer, comparing the bath-exposed ASH with the unexposed ASH remaining within the cuticle. If electrically coupled, the exposed and unexposed ASHs should respond together with minimal lag time; if not coupled, the unexposed ASH should respond much more slowly, as the cuticle remnant will pose a diffusion barrier for the high K^+ buffer. We observed a 5 s delay in the response times of the unexposed ASHs, suggesting a lack of electrical coupling (Fig. 6*D*,*E*). Moreover, the unexposed ASH response times were unaffected by killing the exposed ASH using sharp glass probe, which further confirms the independence of the responses of the two ASH neurons (Fig. 6*F*). Therefore, we do not see evidence for electrical coupling, at least under the conditions we tested. However, the gap junction may be physiologically significant under other conditions because electrical synapses can be dynamically regulated, and therefore may be differentially active under different conditions (Pereda and Macagno, 2017). The proper regulation of ASH response kinetics and/or left-right synchrony appears to be physiologically significant: ASH-specific RNAi inactivation of SLO-1 led to significantly shorter reversal distances following 1-octanol stimulation (as defined as the distance traveled before the first ω turn and/or resumption of forward locomotion) (Fig. 6*G*). Together, our results demonstrate that SLO-1 in ASHs is necessary for 5-HT modulation of aversive behavior, which places SLO-1 in the 5-HT signaling pathway, most likely downstream of Ca^{2+}. However, SLO-1 also plays a role in other important aspects of ASH physiology, including maintenance of resting membrane potential and shaping the response kinetics to aversive odorant stimuli.

Discussion

The objective of this study was to determine how 5-HT signaling in the nociceptive ASH neurons of *C. elegans* can inhibit odorant-evoked Ca^{2+} transients, measured by Ca^{2+} imaging, while potentiating depolarization and aversive behavior. Our results identify a Ca^{2+}-dependent negative feedback pathway in ASHs. 5-HT attenuates this pathway by reducing the Ca^{2+} transient and thereby disinhibiting the ASH response (Fig. 7). This conclusion is based on four principal observations: (1) odorant or high K^+-evoked increases in ASH Ca^{2+} are dependent primarily on an L-type calcium channel, which contains conserved residues for negative regulation by CaN downstream of canonical $G\alpha_q$ signaling, a well-established signaling pathway in other cell types; (2) 5-HT inhibits odorant or high K^+-evoked increases in ASH Ca^{2+} by transiently increasing the release of intracellular Ca^{2+}, via canonical $G\alpha_q$ signaling and subsequent CaN activation; (3) blocking odorant-evoked ASH Ca^{2+} transients potentiates depolarization; and (4) the Ca^{2+}-activated K^+ channel SLO-1 is essential for the 5-HT potentiation of behavior, and profoundly shapes ASH odorant-response kinetics. It is often assumed that Ca^{2+}, entering through voltage-gated Ca^{2+} channels, is the primary carrier of inward current during neuronal depolarization in

C. elegans, which lacks voltage-gated Na^+ channels. However, after blockade of L-type Ca^{2+} channels, we observed no increased Ca^{2+} influx anywhere along the neuron, even though depolarization amplitude increased by 50%. This observation implies that the Ca^{2+} influxes usually measured by Ca^{2+} imaging are unlikely to be the primary carriers of inward current driving depolarization, at least in the ASHs. Instead, we hypothesize that the sensory potential generated by the 1-octanol receptor and downstream transduction pathway is sufficient to depolarize the entire neuron. The sensory transduction pathway activates OSM-9/OCR-2 TRP channels in the cilium (Tobin et al., 2002). TRP channels are generally permeable to Na^+ and Ca^{2+} (Owsianik et al., 2006), and we recorded robust Ca^{2+} transients in the amphids in response to 1-octanol application, regardless of whether the L-type channels were blocked, representing the sensory potential. This depolarization is able to spread passively along the entire length of the ASH neuron to the distal synapses because voltage changes can travel relatively long distances with little to no attenuation in nematode neurons due to their very high membrane resistance (Davis and Stretton, 1989; Goodman et al., 1998). Interestingly, Goodman et al. (1998) also documented counterbalancing Ca^{2+} and K^+ conductances in *C. elegans* neurons, which summed to a 0 net current over a range of physiological potentials (Goodman et al., 1998). L-type Ca^{2+} channels and Ca^{2+}-activated K^+ channels are likely contributors to these currents, based on the conserved roles of these channels in other vertebrate and invertebrate neurons (Gorman et al., 1982; Fettiplace, 1987). 5-HT signaling has the potential to alter this balance by inhibiting Ca^{2+} influx through the L-type channels, thereby reducing the hyperpolarizing K^+ currents and augmenting overall neuronal depolarization.

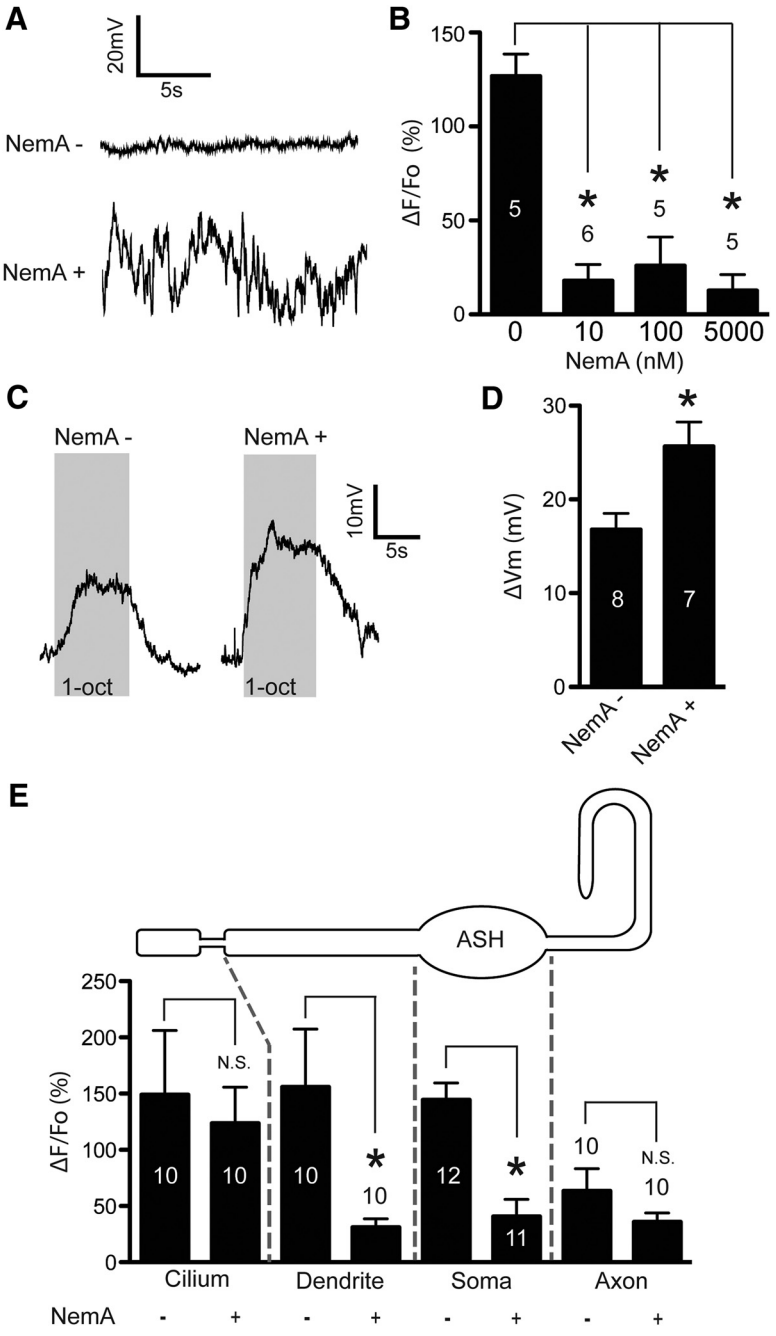

Figure 5. L-type VGCC-dependent Ca^{2+} transients inhibit depolarization. ***A***, Representative trace of the resting membrane potential of an ASH neuron from an untreated worm (top), and a worm incubated on an agar plate containing 5 μM NemA for 45 min (bottom). ***B***, Amplitudes of 1-octanol-evoked Ca^{2+} signals from partially dissected worms treated acutely (1 min) with the indicated concentrations of NemA. *Significantly different from control ($F_{(3,17)} = 22.89$, $p = <0.0001$, ANOVA). ***C***, Representative traces of voltage recordings during 1-octanol stimulation of untreated (left) and worms acutely treated (1 min) with 100 nM NemA (right). Gray boxes represent time of 1-octanol application. ***D***, Amplitudes of 1-octanol-evoked depolarization in untreated and NemA-treated worms (100 nM, 1 min). *Significantly different from control (100 nM treated vs untreated, $p = 0.0185$, $t = 2.761$, df = 11). ***E***, 1-Octanol-evoked Ca^{2+} amplitudes in the cilium, dendrite, soma, and axon (representing the entirety of the cell) in untreated and NemA-treated ASHs. *Significantly different from untreated counterpart. N.S., Not significantly different from untreated counterpart (untreated cilia vs NemA-treated cilia, $p = 0.7024$, $t = 0.3882$, df = 18; untreated dendrite vs NemA-treated dendrite, $p = 0.0277$, $t = 2.395$, df = 18; untreated soma vs NemA-treated soma, $p = <0.0001$, $t = 4.901$, df = 21; untreated axon vs NemA-treated axon, $p = 0.2119$, $t = 1.294$, df = 18). Numbers in/above bars indicate *n*. Data are mean ± SEM.

Regulation of L-type Ca^{2+} channels by GPCRs is widespread and highly conserved. For example, in cardiomyocytes, a conserved serine residue on L-type Ca^{2+} channels is phosphorylated by PKA, and dephosphorylated by CaN, dependent on intracellular Ca^{2+} flowing in through the L-type channel itself (i.e., autoinhibition), and Ca^{2+} released from internal stores. PKA-dependent phosphorylation increases Ca^{2+} currents, leading to increased cardiac output, whereas CaN-dependent dephosphorylation reverses this effect. This mechanism allows bidirectional regulation in the heart, with β-adrenergic signaling increasing cardiac output during times of stress and CaN dephosphorylation providing negative feedback to prevent cardiac muscle overexcitation and damage (Harvey and Hell, 2013). In neurons (both vertebrate and invertebrate), L-type Ca^{2+} channels may be inhibited by GPCRs, including muscarinic acetylcholine,

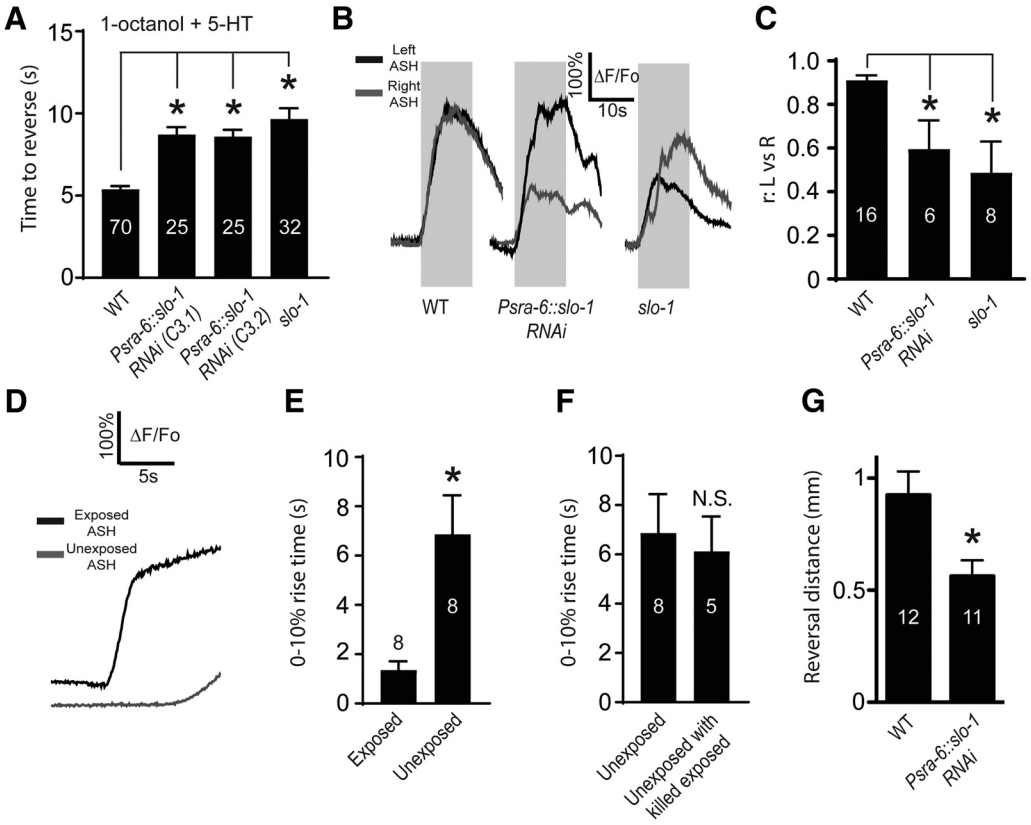

Figure 6. SLO-1 acts downstream of Ca^{2+} in ASHs to regulate 5-HT modulation, ASH-dependent aversive behavior, and ASH response dynamics. ***A***, Reversal times in the 1-octanol avoidance assay, in the presence of 5-HT, for wild-type worms, ASH-specific SLO-1 RNAi knockdown worms (two independent lines, C3.1 and C3.2), and *slo-1* mutants. *Significantly different from control ($F_{(3,136)} = 6.836$, $p < 0.001$, ANOVA). ***B***, Simultaneous Ca^{2+} responses of ASHL and ASHR from individual worms (representative traces). Gray boxes represent 1-octanol application, genotypes, and/or pharmacological treatments indicated below trace. ***C***, Pearson's correlation coefficients (*r*) values for ASHL and ASHR signals. *Significantly different from control ($F_{(2,27)} = 16.87$, $p = 0.0017$, ANOVA). Representative traces (***D***) and 0%–10% rise times (***E***) from simultaneous recordings of exposed and unexposed ASH neurons exposed to high K^+ buffer (see also Materials and Methods; Movie 1). *Significantly different from control (exposed vs unexposed $p = 0.0123$, $t = 3.35$, df = 7, paired *t* test). ***F***, Comparison of 0%–10% rise times from unexposed ASHs in specimens where the exposed ASH was killed. N.S., Not significantly different to control (unexposed rise times reproduced from Fig. 6*E*) ($p = 0.7538$, $t = 0.3216$, df = 11, unpaired *t* test). ***G***, Distance traveled before Ω turn during 1-octanol avoidance, comparing wild-type and ASH-specific SLO-1 RNAi knockdown. *Significantly different from control (*Psra-6::slo-1 RNAi* vs WT, $p = 0.0107$, $t = 2.8$, df = 21). Numbers in bars indicate *n*. Data are mean ± SEM.

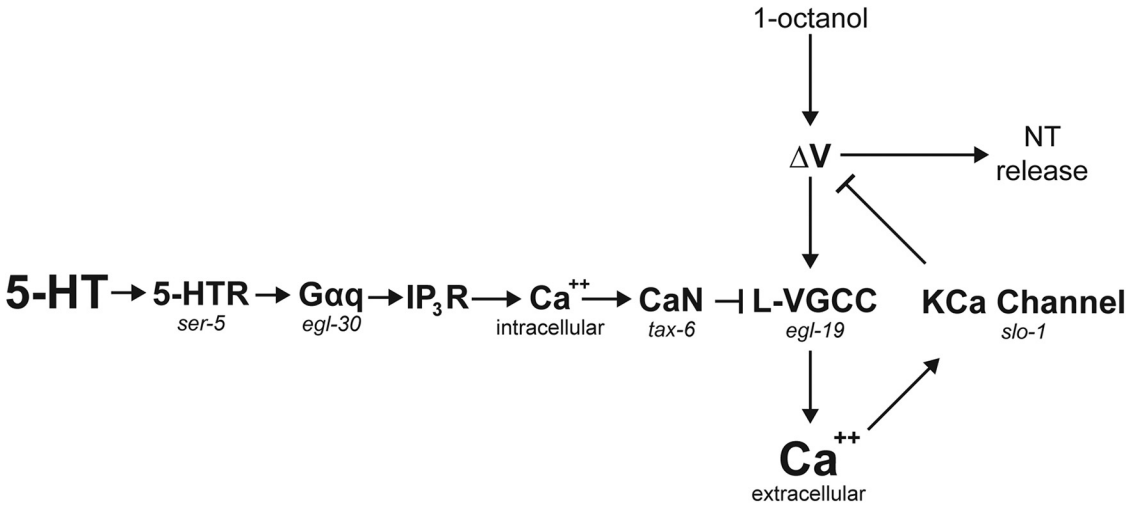

Figure 7. Model for 5-HT disinhibition of ASHs, through modulation of a Ca^{2+}-driven inhibitory feedback loop. Ca^{2+} entry through the L-type VGCC, EGL-19, inhibits ASH excitability by activating the Ca^{2+}-activated K^+ channel SLO-1. 5-HT inhibits the L-VGCC via SER-5, $G\alpha_q$, release of Ca^{2+} from intracellular stores (via the IP_3 receptor), and activation of the CaN ortholog TAX-6, which inhibits EGL-19 by dephosphorylating a highly conserved regulatory Ser residue (based on results reported here; and Zahratka et al., 2015).

5-$HT2_{A/C}$, and DA D2 receptors (Hernandez-Lopez et al., 2000; Day et al., 2002). For 5-HT2 and D2 signaling, the involvement of IP_3R-mediated Ca^{2+} release and CaN activation has been documented (Hernandez-Lopez et al., 2000; Day et al., 2002), similar to the results described here. Similarly, the association of L-type Ca^{2+} channels and Ca^{2+}-activated K^+ channels is highly conserved and well documented. These channels function together in many contexts, including regulation of secretion and synaptic release, setting the membrane potential, and modulating electrical excitability (Lewis and Hudspeth, 1983; Goodman et al., 1998; Vandael et al., 2010; Steciuk et al., 2014; Contet et al., 2016) and, moreover, physically associate in signaling complexes (Kim et al., 2009; Chen et al., 2010, 2011; Kim and Oh 2016). The novel aspect of the present study is to connect 5-HT receptor signaling, CaN-dependent regulation of L-type Ca^{2+} channels, Ca^{2+}-dependent modulation of depolarization, and Ca^{2+}-activated K^+ channels in a single pathway that modulates the electrical excitability of a sensory neuron, and its corresponding sensory-mediated behavior. We also observed an unexpected, but critical, role for SLO-1 in precisely shaping the response kinetics of ASHs. Loss of SLO-1 in ASHs leads to highly variable response profiles, loss of synchrony between the ASHL and ASHR, and defective overall avoidance behavior.

In this study, we emphasized a pharmacological method for studying ASH physiology, in which we gently exposed the ASH soma to the bath by partial dissection while maintaining its dendritic connection to the amphid and preserving functionality. By precisely controlling liquid flow, we could independently target the amphid openings and neuronal soma with different solutions (e.g., odorants and neurotransmitters/drugs, respectively) without cross-contamination. This approach greatly improved the accessibility of the ASH to modulatory ligands by removing the relatively impermeable nematode cuticle as a barrier, leading to several important insights. For example, we demonstrated that 5-HT modulation takes place at physiological concentration ranges (i.e., nM). In contrast, effective concentrations have been impossible to quantify or precisely control using previous approaches in *C. elegans*, where intact worms are soaked in high concentrations of monoamines (i.e., mM) for upward of 30 min (Horvitz et al., 1982; Chao et al., 2004; Harris et al., 2009, 2011; Ezcurra et al., 2011; Ghosh et al., 2016). The rapidity of ligand application in our dissected preparations was also advantageous. Under these conditions, the very early rise in intracellular Ca^{2+} downstream of SER-5 activation by 5-HT was detectable, and we could thereby define two separate ASH Ca^{2+} pools with distinct origins and functions. Acute ligand application also mitigates the potential for indirect effects to confound data interpretation. Observed effects are less likely to be the result of secondary signaling by another cell type because of the short time frame. Moreover, the exposed cell soma and applied ligand are largely isolated from the remainder of the *C. elegans* nervous system, further reducing the potential for non–cell-autonomous signaling mechanisms to operate. Over longer time frames, developmental and physiological compensation can significantly confound experimental analysis. We encountered examples of this with *slo-1* mutants and cell-specific RNAi knockdown, and 45 min incubation of worms on NemA-containing plates, which were overcome using the acute application approach. These observations demonstrate that acute direct application of agonists, antagonists, neurotransmitters, and neuropeptides to dissected neural soma can produce critical insights into the biochemical basis of neural circuit function in the *C. elegans* model.

In conclusion, our results have important implications for interpreting Ca^{2+} imaging data in neural circuit analysis. Ca^{2+} transients are often treated quantitatively, with the amplitude of the Ca^{2+} signal assumed to positively correlate with the strength of the membrane depolarization (Shidara et al., 2013; Kato et al., 2014; Guo et al., 2015; Ghosh et al., 2016; Gourgou and Chronis, 2016; Chen et al., 2017). Our results challenge this view by demonstrating that, in the ASH neurons, Ca^{2+} transient and depolarization amplitudes change in opposite directions in response to 5-HT signaling, that GPCR signaling can dramatically modulate Ca^{2+} signal strength independently of depolarization, that GPCR signaling can elicit measurable Ca^{2+} signals from internal stores in the absence of depolarization, and that Ca^{2+} can act as second messenger to significantly reduce membrane depolarization (current study; Zahratka et al., 2015). These observations show that the relationship between Ca^{2+} signals and the membrane potential is not necessarily monotonic. Instead, Ca^{2+} signals contain a wealth of information about a neuron's physiological state and neuromodulatory milieu. These observations are relevant not only to *C. elegans* circuit analysis, where neurons rely on graded potentials rather than action potentials (Goodman et al., 1998), but also to other experimental systems, where action potential frequency must be calculated from neuronal Ca^{2+} signal amplitudes using computer algorithms (Sasaki et al., 2008; Vogelstein et al., 2009).

References

Adolph AR, Tuan FJ (1972) Serotonin and inhibition in limulus lateral eye. J Gen Physiol 60:679–697. CrossRef Medline

Alqadah A, Hsieh YW, Schumacher JA, Wang X, Merrill SA, Millington G, Bayne B, Jorgensen EM, Chuang CF (2016) SLO BK potassium channels couple gap junctions to inhibition of calcium signaling in olfactory neuron diversification. PLoS Genet 12:e1005654. CrossRef Medline

Baker KD, Edwards TM, Rickard NS (2013) The role of intracellular calcium stores in synaptic plasticity and memory consolidation. Neurosci Biobehav Rev 37:1211–1239. CrossRef Medline

Bandyopadhyay J, Lee J, Lee J, Lee JI, Yu JR, Jee C, Cho JH, Jung S, Lee MH, Zannoni S, Singson A, Kim DH, Koo HS, Ahnn J (2002) Calcineurin, a calcium/calmodulin-dependent protein phosphatase, is involved in movement, fertility, egg laying, and growth in *Caenorhabditis elegans*. Mol Biol Cell 13:3281–3293. CrossRef Medline

Blaich A, Pahlavan S, Tian Q, Oberhofer M, Poomvanicha M, Lenhardt P, Domes K, Wegener JW, Moosmang S, Ruppenthal S, Scholz A, Lipp P, Hofmann F (2012) Mutation of the calmodulin binding motif IQ of the L-type Ca(v)1.2 Ca^{2+} channel to EQ induces dilated cardiomyopathy and death. J Biol Chem 287:22616–22625. CrossRef Medline

Bunin MA, Wightman RM (1998) Quantitative evaluation of 5-hydroxytryptamine (serotonin) neuronal release and uptake: an investigation of extrasynaptic transmission. J Neurosci 18:4854–4860. Medline

Chao MY, Komatsu H, Fukuto HS, Dionne HM, Hart AC (2004) Feeding status and serotonin rapidly and reversibly modulate a *Caenorhabditis elegans* chemosensory circuit. Proc Natl Acad Sci U S A 101:15512–15517. CrossRef Medline

Chase DL, Koelle MR (2007) Biogenic amine neurotransmitters in *C. elegans*. WormBook 20:1–15. CrossRef Medline

Chen B, Ge Q, Xia XM, Liu P, Wang SJ, Zhan H, Eipper BA, Wang ZW (2010) A novel auxiliary subunit critical to BK channel function in *Caenorhabditis elegans*. J Neurosci 30:16651–16661. CrossRef Medline

Chen B, Liu P, Zhan H, Wang ZW (2011) Dystrobrevin controls neurotransmitter release and muscle Ca(2+) transients by localizing BK channels in *Caenorhabditis elegans*. J Neurosci 31:17338–17347. CrossRef Medline

Chen C, Itakura E, Nelson GM, Sheng M, Laurent P, Fenk LA, Butcher RA, Hegde RS, de Bono M (2017) IL-17 is a neuromodulator of *Caenorhabditis elegans* sensory responses. Nature 542:43–48. CrossRef Medline

Chiechio S (2016) Modulation of chronic pain by metabotropic glutamate receptors. Adv Pharmacol 75:63–89. CrossRef Medline

Contet C, Goulding SP, Kuljis DA, Barth AL (2016) BK channels in the

central nervous system. Int Rev Neurobiol 128:281–342. CrossRef Medline

Davis RE, Stretton AO (1989) Passive membrane properties of motorneurons and their role in long-distance signaling in the nematode ascaris. J Neurosci 9:403–414. Medline

Day M, Olson PA, Platzer J, Striessnig J, Surmeier DJ (2002) Stimulation of 5-HT(2) receptors in prefrontal pyramidal neurons inhibits Ca(v)1.2 L type Ca(2+) currents via a PLCbeta/IP_3/calcineurin signaling cascade. J Neurophysiol 87:2490–2504. CrossRef Medline

Donohoe DR, Jarvis RA, Weeks K, Aamodt EJ, Dwyer DS (2009) Behavioral adaptation in *C. elegans* produced by antipsychotic drugs requires serotonin and is associated with calcium signaling and calcineurin inhibition. Neurosci Res 64:280–289. CrossRef Medline

Esposito G, Di Schiavi E, Bergamasco C, Bazzicalupo P (2007) Efficient and cell specific knock-down of gene function in targeted *C. elegans* neurons. Gene 395:170–176. CrossRef Medline

Ezcurra M, Tanizawa Y, Swoboda P, Schafer WR (2011) Food sensitizes *C. elegans* avoidance behaviours through acute dopamine signalling. EMBO J 30:1110–1122. CrossRef Medline

Fettiplace R (1987) Electrical tuning of hair cells in the inner ear. Trends Neurosci 10:421–425. CrossRef

Ghosh DD, Sanders T, Hong S, McCurdy LY, Chase DL, Cohen N, Koelle MR, Nitabach MN (2016) Neural architecture of hunger-dependent multisensory decision making in *C. elegans*. Neuron 92:1049–1062. CrossRef Medline

Goodman MB, Lockery SR (2000) Pressure polishing: a method for reshaping patch pipettes during fire polishing. J Neurosci Methods 100:13–15. CrossRef Medline

Goodman MB, Hall DH, Avery L, Lockery SR (1998) Active currents regulate sensitivity and dynamic range in *C. elegans* neurons. Neuron 20:763–772. CrossRef Medline

Gorman AL, Hermann A, Thomas MV (1982) Ionic requirements for membrane oscillations and their dependence on the calcium concentration in a molluscan pace-maker neurone. J Physiol 327:185–217. CrossRef Medline

Gourgou E, Chronis N (2016) Chemically induced oxidative stress affects ASH neuronal function and behavior in *C. elegans*. Sci Rep 6:38147. CrossRef Medline

Guo M, Wu TH, Song YX, Ge MH, Su CM, Niu WP, Li LL, Xu ZJ, Ge CL, Al-Mhanawi MT, Wu SP, Wu ZX (2015) Reciprocal inhibition between sensory ASH and ASI neurons modulates nociception and avoidance in *Caenorhabditis elegans*. Nat Commun 6:5655. CrossRef Medline

Gutierrez GJ, Marder E (2014) Modulation of a single neuron has state-dependent actions on circuit dynamics. eNeuro 1:1. CrossRef Medline

Harris GP, Hapiak VM, Wragg RT, Miller SB, Hughes LJ, Hobson RJ, Steven R, Bamber B, Komuniecki RW (2009) Three distinct amine receptors operating at different levels within the locomotory circuit are each essential for the serotonergic modulation of chemosensation in *Caenorhabditis elegans*. J Neurosci 29:1446–1456. CrossRef Medline

Harris G, Korchnak A, Summers P, Hapiak V, Law WJ, Stein AM, Komuniecki P, Komuniecki R (2011) Dissecting the serotonergic food signal stimulating sensory-mediated aversive behavior in *C. elegans*. PLoS One 6:e21897. CrossRef Medline

Harris-Warrick RM, Johnson BR (2010) Checks and balances in neuromodulation. Front Behav Neurosci 4:1–9. CrossRef Medline

Harvey RD, Hell JW (2013) CaV1.2 signaling complexes in the heart. J Mol Cell Cardiol 58:143–152. CrossRef Medline

Hernandez-Lopez S, Tkatch T, Perez-Garci E, Galarraga E, Bargas J, Hamm H, Surmeier DJ (2000) D2 dopamine receptors in striatal medium spiny neurons reduce L-type Ca^{2+} currents and excitability via a novel PLC[beta]1-IP_3-calcineurin-signaling cascade. J Neurosci 20:8987–8995. Medline

Hobert O (2010) Neurogenesis in the nematode *Caenorhabditis elegans*. WormBook 4:1–24. CrossRef Medline

Hogan QH (2007) Role of decreased sensory neuron membrane calcium currents in the genesis of neuropathic pain. Croat Med J 48:9–21. Medline

Horvitz HR, Chalfie M, Trent C, Sulston JE, Evans PD (1982) Serotonin and octopamine in the nematode *Caenorhabditis elegans*. Science 216:1012–1014. CrossRef Medline

Kato S, Xu Y, Cho CE, Abbott LF, Bargmann CI (2014) Temporal responses of *C. elegans* chemosensory neurons are preserved in behavioral dynamics. Neuron 81:616–628. CrossRef Medline

Kato S, Kaplan HS, Schrödel T, Skora S, Lindsay TH, Yemini E, Lockery S, Zimmer M (2015) Global brain dynamics embed the motor command sequence of *Caenorhabditis elegans*. Cell 163:656–669. CrossRef Medline

Kim H, Oh KH (2016) Protein network interacting with BK channels. Int Rev Neurobiol 128:127–161. CrossRef Medline

Kim H, Pierce-Shimomura JT, Oh HJ, Johnson BE, Goodman MB, McIntire SL (2009) The dystrophin complex controls bk channel localization and muscle activity in *Caenorhabditis elegans*. PLoS Genet 5:e1000780. CrossRef Medline

Koelle MR (2016) Neurotransmitter signaling through heterotrimeric G proteins: insights from studies in *C. elegans*. WormBook 3:1–78. CrossRef Medline

Kuhara A, Inada H, Katsura I, Mori I (2002) Negative regulation and gain control of sensory neurons by the *C. elegans* calcineurin TAX-6. Neuron 33:751–763. CrossRef Medline

Lemon WC, Pulver SR, Höckendorf B, McDole K, Branson K, Freeman J, Keller PJ (2015) Whole-central nervous system functional imaging in larval *Drosophila*. Nat Commun 6:7924. CrossRef Medline

Lewis RS, Hudspeth AJ (1983) Voltage- and ion-dependent conductances in solitary vertebrate hair cells. Nature 304:538–541. CrossRef Medline

Marder E (2012) Neuromodulation of neuronal circuits: back to the future. Neuron 76:1–11. CrossRef Medline

McCreary AC, Newman-Tancredi A (2015) Serotonin 5-HT1A receptors and antipsychotics- an update in light of new concepts and drugs. Curr Pharm Des 21:3725–3731. CrossRef Medline

Miller KG, Emerson MD, Rand JB (1999) Goalpha and diacylglycerol kinase negatively regulate the gqalpha pathway in *C. elegans*. Neuron 24:323–333. CrossRef Medline

Mills H, Wragg R, Hapiak V, Castelletto M, Zahratka J, Harris G, Summers P, Korchnak A, Law W, Bamber B, Komuniecki R (2012) Monoamines and neuropeptides interact to inhibit aversive behaviour in *Caenorhabditis elegans*. EMBO J 31:667–678. CrossRef Medline

Nadim F, Bucher D (2014) Neuromodulation of neurons and synapses. Curr Opin Neurobiol 29:48–56. CrossRef Medline

Naumann EA, Fitzgerald JE, Dunn TW, Rihel J, Sompolinsky H, Engert F (2016) From whole-brain data to functional circuit models: the zebrafish optomotor response. Cell 167:947–960.e20. CrossRef Medline

Oh WC, Song HO, Cho JH, Park BJ (2011) ANK repeat-domain of SHN-1 is indispensable for in vivo SHN-1 function in *C. elegans*. Mol Cells 31:79–84. CrossRef Medline

Oliveria SF, Dittmer PJ, Youn DH, Dell'Acqua ML, Sather WA (2012) Localized calcineurin confers Ca^{2+}-dependent inactivation on neuronal L-type Ca^{2+} channels. J Neurosci 32:15328–15337. CrossRef Medline

Olson PA, Tkatch T, Hernandez-Lopez S, Ulrich S, Ilijic E, Mugnaini E, Zhang H, Bezprozvanny I, Surmeier DJ (2005) G-protein-coupled receptor modulation of striatal CaV1.3 L-type Ca^{2+} channels is dependent on a shank-binding domain. J Neurosci 25:1050–1062. CrossRef Medline

Owsianik G, Talavera K, Voets T, Nilius B (2006) Permeation and selectivity of TRP channels. Annu Rev Physiol 68:685–717. CrossRef Medline

Pereda AE, Macagno E (2017) Electrical transmission: two structures, same functions? Dev Neurobiol 77:517–521. CrossRef Medline

Poort J, Khan AG, Pachitariu M, Nemri A, Orsolic I, Krupic J, Bauza M, Sahani M, Keller GB, Mrsic-Flogel TD, Hofer SB (2015) Learning enhances sensory and multiple non-sensory representations in primary visual cortex. Neuron 86:1478–1490. CrossRef Medline

Ransdell JL, Nair SS, Schulz DJ (2012) Rapid homeostatic plasticity of intrinsic excitability in a central pattern generator network stabilizes functional neural network output. J Neurosci 32:9649–9658. CrossRef Medline

Sasaki T, Takahashi N, Matsuki N, Ikegaya Y (2008) Fast and accurate detection of action potentials from somatic calcium fluctuations. J Neurophysiol 100:1668–1676. CrossRef Medline

Shidara H, Kobayashi J, Tanamoto R, Hotta K, Oka K (2013) Odorant-induced membrane potential depolarization of AIY interneuron in *Caenorhabditis elegans*. Neurosci Lett 541:199–203. CrossRef Medline

Singer WD, Brown HA, Sternweis PC (1997) Regulation of eukaryotic phosphatidylinositol-specific phospholipase C and phospholipase D. Annu Rev Biochem 66:475–509. CrossRef Medline

Steciuk M, Cheong M, Waite C, You YJ, Avery L (2014) Regulation of synaptic transmission at the *Caenorhabditis elegans* M4 neuromuscular junction by an antagonistic relationship between two calcium channels. G3 (Bethesda) 4:2535–2543. CrossRef Medline

Stein C, Zollner C (2009) Opioids and sensory nerves. Handb Exp Pharmacol 194:495–518. CrossRef Medline

Stevens TR, Krueger SR, Fitzsimonds RM, Picciotto MR (2003) Neuroprotection by nicotine in mouse primary cortical cultures involves activation of calcineurin and L-type calcium channel inactivation. J Neurosci 23: 10093–10099. Medline

Stoop R (2014) Neuromodulation by oxytocin and vasopressin in the central nervous system as a basis for their rapid behavioral effects. Curr Opin Neurobiol 29:187–193. CrossRef Medline

Swensen AM, Marder E (2001) Modulators with convergent cellular actions elicit distinct circuit outputs. J Neurosci 21:4050–4058. Medline

Tobin DM, Madsen DM, Kahn-Kirby A, Peckol EL, Moulder G, Barstead R, Maricq AV, Bargmann CI (2002) Combinatorial expression of TRPV channel proteins defines their sensory functions and subcellular localization in *C. elegans* neurons. Neuron 35:307–318. CrossRef Medline

Vandael DH, Marcantoni A, Mahapatra S, Caro A, Ruth P, Zuccotti A, Knipper M, Carbone E (2010) Ca(v)1.3 and BK channels for timing and regulating cell firing. Mol Neurobiol 42:185–198. CrossRef Medline

Vogelstein JT, Watson BO, Packer AM, Yuste R, Jedynak B, Paninski L (2009) Spike inference from calcium imaging using sequential Monte Carlo methods. Biophys J 97:636–655. CrossRef Medline

Vogt N (2015) Voltage sensors: challenging, but with potential. Nat Methods 12:921–924. CrossRef Medline

Walker DS, Vázquez-Manrique RP, Gower NJ, Gregory E, Schafer WR, Baylis HA (2009) Inositol 1,4,5-trisphosphate signalling regulates the avoidance response to nose touch in *Caenorhabditis elegans*. PLoS Genet 5:e1000636. CrossRef Medline

Wang Y, Tandan S, Hill JA (2014) Calcineurin-dependent ion channel regulation in heart. Trends Cardiovasc Med 24:14–22. CrossRef Medline

Wang ZW, Saifee O, Nonet ML, Salkoff L (2001) SLO-1 potassium channels control quantal content of neurotransmitter release at the *C. elegans* neuromuscular junction. Neuron 32:867–881. CrossRef Medline

White JG, Southgate E, Thomson JN, Brenner S (1986) The structure of the nervous system of the nematode *Caenorhabditis elegans*. Philos Trans R Soc Lond B Biol Sci 314:1–340. CrossRef Medline

Yohn CN, Gergues MM, Samuels BA (2017) The role of 5-HT receptors in depression. Mol Brain 10:28. CrossRef Medline

Zahratka JA, Williams PD, Summers PJ, Komuniecki RW, Bamber BA (2015) Serotonin differentially modulates Ca^{2+} transients and depolarization in a *C. elegans* nociceptor. J Neurophysiol 113:1041–1050. CrossRef Medline